Crystal Engineering

DOI: 10.1002/ange.201002558

Self-Assembly of Nanotriangle Superlattices Facilitated by Repulsive Electrostatic Interactions**

*David A. Walker, Kevin P. Browne, Bartlomiej Kowalczyk, and Bartosz A. Grzybowski**

Self-assembly of nanoscopic components into ordered "supra-structures" is a promising route to new types of nanomaterials with applications in catalysis,[1] optoelectronics,[2] and biological sensing,[3] to name just a few. Whereas numerous strategies (mostly, evaporation-driven[4–8] but also based on electrostatic interactions[9–12] or DNA base-pairing[13]) have been developed to crystallize spherical particles into large two-dimensional lattices and three-dimensional crystals, the self-assembly of components of lower symmetries (rods, plates, etc.[14]) remains challenging. For such particles, crystallization is often hindered by strong van der Waals (vdW) attractions,[15] which lead to indiscriminate "sticking" of the particles rather than to orientation-specific self-assembly. Several groups[4,5] have recently demonstrated the assembly of nanorods (with the help of cationic or Gemini surfactants) and of columnar structures made of platelets[6,16] (where entropic forces[15] facilitate organization at high volume fractions), but crystallization of high-aspect ratio (width: thickness) polygonal nanocrystals has not been reported. Such polygons—especially, metallic nanotriangles—and their arrays are of particular interest because of the presence of sharp edges, where electromagnetic fields are concentrated into "hot-spots" which enhance SERS (surface-enhanced Raman spectroscopy) sensing abilities.[17–21] Herein, we demonstrate the assembly of metallic nanotriangles (NTs) into ordered monolayer and multilayer structures. The remarkable feature of this method is that self-assembly is facilitated by repulsive electrostatic interactions between the triangles introduced by charged surfactants.[22] These repulsions weaken the strong vdW attractions between the flat faces of the triangles and effectively serve as a "molecular lubricant" that allows the particles to fine-tune their mutual orientations. Confocal Raman imaging shows that ordering of the metallic triangles into large arrays enhances Raman scattering and significantly increases the SERS sensitivity relative to randomly aggregated NTs. In a general context, the use of repulsive forces appears a versatile strategy for "softening" strong attractive potentials in self-assembling systems at the nanoscale.

Approximately equilateral nanotriangles (NTs; side $a = 158 \pm 14$ nm; thickness $h = 8.7 \pm 0.8$ nm; Figure 1 a,b), were synthesized by sequential seeded growth from citrate-stabilized gold seeds (see the Experimental Section and reference [25]). The as-synthesized AuNTs were then purified by two sedimentation and redispersion steps with fresh deionized water to remove excess hexadecyltrimethylammonium bromide (CTAB) surfactant as well as isotropic side-products. The purified NTs, stabilized by CTAB, were subsequently functionalized with self-assembled monolayers (SAMs) of *N*,*N*,*N*-trimethyl(11-mercaptoundecyl)ammonium chloride (TMA, ProChimia, Poland), which displaces the CTAB surfactant.

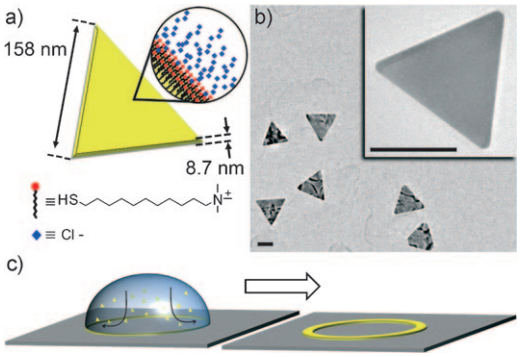

Figure 1. a) Sketch and dimensions of gold nanotriangles functionalized with TMA thiols. Cl^- counterions are shown as blue diamonds. b) Representative TEM image of TMA-functionalized AuNTs. Inset: Individual NT at higher magnification. Scale bars = 100 nm. c) Illustration of the experiment in which evaporation of a droplet containing NTs leaves behind a "pinned" ring of organized nanotriangles. Arrows within the droplet indicate the direction of convective flows as previously reported in references [23, 24].

In a typical experiment, self-assembly was achieved by placing a 4 μL droplet of the NT solution (ca. 10^{10} NTs mL^{-1}) on a solid substrate. The specific substrates tested were 1) monocrystalline {100} silicon wafers, 2) oxidized silicon wafers (Si/SiO_2), 3) gold-coated silicon wafers functionalized with a positively charged TMA SAM, and 4) gold-coated silicon wafers functionalized with deprotonated, negatively charged mercaptoundeconoic acid (MUA) SAM. On each of these surfaces, a droplet of NT solution was left to evaporate

[*] D. A. Walker,[+] K. P. Browne,[+] Dr. B. Kowalczyk, Prof. B. A. Grzybowski
Department of Chemical and Biological Engineering, Department of Chemistry, Northwestern University
2145 Sheridan Rd., Tech E136, Evanston, IL 60208 (USA)
E-mail: grzybor@northwestern.edu
Homepage: http://dysa.northwestern.edu/

[+] These authors contributed equally.

[**] This work was supported by the Non-equilibrium Energy Research Center (NERC), which is an Energy Frontier Research Center funded by the U.S. Department of Energy, Office of Science, Office of Basic Energy Sciences under Award Number DE-SC0000989 (K.P.B., B.K., and B.A.G.). The work was also supported by the Materials Research Science and Engineering Center (MRSEC) funded by the National Science Foundation under NSF Award Number DMR-0520513 (D.A.W.).

under ambient conditions. This simple yet popular evaporation technique[4,5,24,26]—one in which convective flows and contact-line-pinning[23,24] are thought to help preconcentrate the crystallizing objects—resulted in the formation of NT aggregates from the perimeter of the drying droplet inwards (Figure 1c).

The morphology of the NT aggregates depended predominantly on the functionalization of the NTs. When the triangles were stabilized by CTAB surfactant (up to ca. 20 mM)[27] alone, they formed random aggregates rather than ordered assemblies (Figure 2a). The formation of

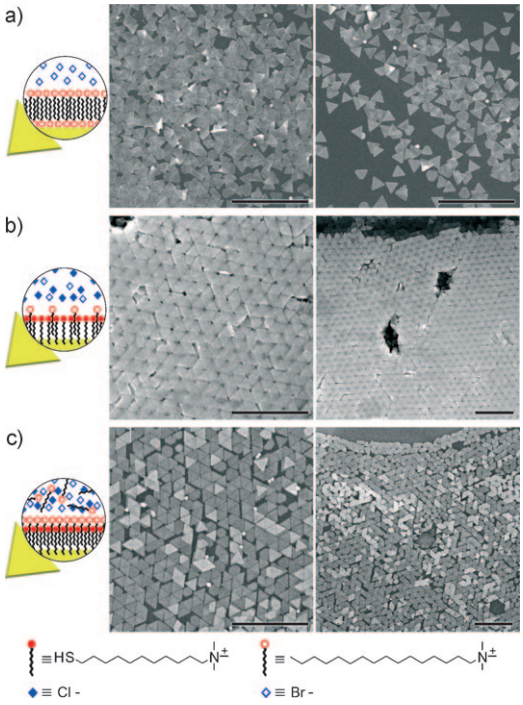

Figure 2. a) AuNTs stabilized only by excess CTAB surfactant (20 mM CTAB, $\varphi_o = 35$ mV, $E_{el} \approx 330\,kT$) form disordered aggregates. b) Triangles functionalized with TMA surfactants and with only residual CTAB surfactant present (< 1 mM CTAB, $\varphi_o = 60$ mV, $E_{el} \approx 960\,kT$) organize into large, ordered multilayers. c) AuNTs stabilized with TMA SAMs and in the presence of excess CTAB (20 mM CTAB, $\varphi_o = 79$ mV, $E_{el} \approx 2300\,kT$) give large monolayer arrays. All scale bars = 1 μm.

ordered lattices required the NTs to be coated with covalently linked charged molecules—in our case, SAMs of positively charged TMA thiols.[28] For TMA NTs with only residual CTAB (< 1 mM) remaining after postsynthesis washings, the triangles organized into large crystalline aggregates approximately 4–6 layers thick (Figure 2b) and with a total area of approximately 40,000 μm^2 (note: the area of one NT is around 0.011 μm^2). In contrast, the simultaneous use of both covalently bound TMA and excess CTAB in solution led to the formation of large, approximately 55 000 μm^2 NT monolayers.

For both multi- and monolayer NT arrays, the properties of the material and the charge of the supporting material (i.e., Si, SiO_2, AuTMA, AuMUA) had no noticeable effect on the structures of NT assemblies. It follows that NT ordering depends predominantly on the interactions between the triangles. Although exact calculations of free energies (i.e., including entropic effects) are prohibitively complicated, the experimentally observed trends can be rationalized on the basis of the interplay between van der Waals (vdW) attractions and electrostatic repulsions. The vdW forces scale approximately with the area of contact and are strongest when the NTs are stacked "on top" of one another. The energy of these interactions can be estimated using the Hamaker integral approximation[15] for two flat plates of finite thickness. The vdW energy per unit area is given by $E_{vdW} = -A\left[1/d^2 - 2/(d+h)^2 + 1/(d+2h)^2\right]/12\pi$,[29] where $A \approx 10^{-19}$ J[30] is the Hamaker constant for gold across water, d is the distance between the two plates (in this case, about twice the SAM thickness, ca. 2.8 nm[10]), and $h \approx 8.7$ nm is the thickness of the plates. For the NTs we used, the maximal surface area of contact (when two triangles are stacked perfectly) was 11 000 nm^2, and the corresponding value of E_{vdw} was $-820\,kT$. In the absence of other interactions, such magnitudes are more than enough to cause particle aggregation and overcome any entropic "penalties" caused by the loss of translational and rotational degrees of freedom incurred during the process.[15] In our experiments, however, these attractions can be counterbalanced by electrostatic repulsions. The electrostatic energy, per unit area, between two semi-infinite plates with equivalent potentials is[31] $E_{el} = \varepsilon\varepsilon_o\kappa\phi_o^2(1 - \tan(\kappa d/2))$, where $\varepsilon_o$is the permittivity of free space, ε is the relative permittivity of the solvent (in this case, water), κ^{-1} is the electrostatic screening length, and φ_o is the constant potential at the plate's surface.[32] To determine φ_o, we solved the boundary-value problem described by the linearized Poisson–Boltzman (PB) equation, $\nabla^2\varphi = \kappa^2\varphi$, where the relation between charge density and potential, $\sigma = d\varphi_o/dx$, can be applied at the boundaries $x = 0$ and $x = d$ (coordinate x is perpendicular to the plates' surfaces). Solving the equation yields $\sigma = \varepsilon\kappa\varphi_o(\coth(\kappa d) - \operatorname{csch}(\kappa d))$, which relates the surface potential to the charge density (which was determined from electrophoretic mobility experiments[33]). Once the surface potential of the particles is known, the electrostatic energy of assembly can be calculated.

For NTs stabilized by CTAB, the surface potential we determined, $\varphi_o = 35$ mV, agrees with previously reported values and, through the formalism developed above, gives the energy of electrostatic repulsion $E_{el} \approx 330\,kT$, which is smaller than the value of E_{vdw}—consequently, the process of assembly is dominated by the vdW forces, leading to rapid and indiscriminate aggregation. This situation changes for TMA-functionalized NTs, which, in the presence of residual CTAB, have $\varphi_o = 60$ mV such that $E_{el} \approx 960\,kT$ is comparable with the value of E_{vdw}. In this case, it is the balance between attractions and repulsions that controls self-assembly and allows the NTs to adjust their mutual orientations during the crystallization process and form well-ordered, multilayer structures. Finally, the surface potential is the highest ($\varphi_o =$ 79 mV) for TMA-functionalized NTs in the presence of excess surfactant (which can, in principle, intercalate into the TMA SAM and increase its charge; see inset in Figure 2c). In this case, $E_{el} \approx 2300\,kT > E_{vdW}$, and the interaction between the NTs is repulsive such that stacking of the triangles into multilayers is energetically unfavorable. At the same time, the

triangles are large and massive enough that they sediment from solution[34] onto the deposition substrate where they form monolayers. Of course, details of this process are likely to be more complex and may involve drying effects.

One of the main motivations for the preparation of nanotriangle arrays (usually, via lithography[35]) is their use in SERS, because the electromagnetic fields between the tips of adjacent triangles are enhanced.[36–38] We used confocal Raman spectroscopy to map out these enhancement effects and investigate the SERS performance of crystalline NT assemblies (Figure 3). NT crystals were prepared identically to those discussed earlier, with the exception that a small amount (5 μM) of methylene blue (MB) was added to the NT solution. MB was previously used to map Raman hotspots of round nanodisks,[39] whereby its intense C–C ring stretching mode at 1621 cm^{-1} was monitored. Our samples were excited with a He–Ne laser (633 nm) with a spot size of approximately 1 μm and power density of around 3×10^4 W/cm^2. Raman maps (Figure 3b,d) with a scan range of 10×10 μm (100 pixels × 100 lines) were collected by taking a complete Raman spectrum at every pixel with an integration time of 1 sec, and integrating the counts recorded for the C–C ring-stretching peak.

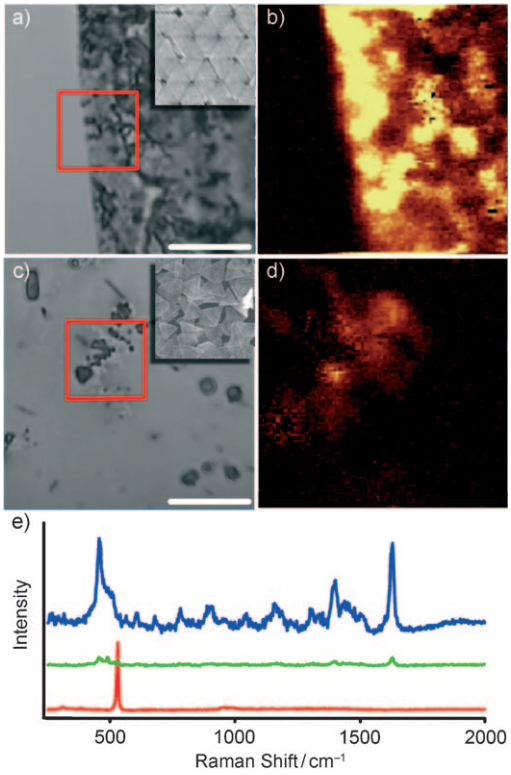

Figure 3. a) Optical microscopy image and b) confocal Raman mapping of ordered NT crystals. The inset in (a) is a representative SEM image of an ordered NT array, and the red box defines the region over which the Raman map (b) was collected. c) Optical microscopy image and d) confocal Raman mapping of randomly assembled NT aggregates. The inset in (c) is a representative SEM image of the orderless NT aggregates, and the red box defines the region over which the Raman map (d) was collected. Scale bars in optical images are 10 μm. Both Raman maps are 10 μm by 10 μm (100 by 100 pixels); each pixel is the integration of the MB peak located at around 1620 cm^{-1}. e) Raman spectra collected for MB on an ordered NT crystal (blue spectrum; 1 s integration time) shows enhancement an order of magnitude larger than enhancement of MB peaks by disordered NT aggregates (green spectrum; 1 s integration time). In the absence of NTs, there is no enhancement of the MB peaks (red spectrum; 30 s integration time), and only the Si peak (from the substrate) is observed (ca. 600 cm^{-1}). Each spectrum is baseline-corrected and offset for clarity.

An optical microscopy image (Figure 3a) and a confocal Raman map of an MB-laced NT multilayer crystal (Figure 3b) illustrate that intense enhancement is observed over the crystal's surface while the surrounding bare Si surface (with identical MB concentration and even with much longer integration times) shows no enhancement. Although these observations prove that NT assemblies are SERS-active, they do not per se demonstrate that ordering enhances the signal relative to that of the individual NTs. Therefore, to gauge the influence of crystalline ordering on SERS enhancement, additional confocal Raman maps were collected of randomly assembled, CTAB-stabilized NT aggregates with similar NT densities and MB concentrations (Figure 3c,d). Under these conditions, the intensities of the MB peaks were enhanced relativce to regions where no nanotriangles were present but were approximately one order of magnitude less than the intensities of peaks recorded over NT crystals. From these experiments—quantified in the form of Raman spectra such as those in Figure 3e—we conclude that assembling the NTs into crystals leads to a significant SERS enhancement,[40] likely as a result of having the tips of many NTs locally concentrated to within few tens of square nanometers.

In summary, we have described the assembly of nanotriangular prisms into close-packed, mono- and multilayer arrays. Paradoxically, our method's success rests on adjusting the repulsive interactions between the assembling particles. The use of electrostatic repulsions to weaken interparticle interactions appears to be a novel strategy of "softening" interparticle potentials in cases where all-attractive forces favor the formation of orderless aggregates rather than ordered assemblies. The specific nanotriangular structures we described can provide the basis for SERS-based sensing platforms, where the precise ordering and alignment within the array leads to an additional, order-of-magnitude increase in SERS sensing capabilities.

Experimental Section

NTs were synthesized from citrate-stabilized seed particles as reported by Mirkin and co-workers.[25] The concentration of iodide ions was controlled by purifying the as-received CTAB through multiple recrystallizations and then adding a controlled amount of KI (see references [25,41] for discussion of variations in CTAB from batch to batch and how this plays a large role in nanosynthesis). Following synthesis, NTs were purified by sedimenting overnight in a 28 °C water bath (to prevent CTAB from precipitating out of solution). The supernatant (pink, containing predominately isotropic products) was removed and the precipitated NTs were redispersed in deionized water. This sedimentation and redispersion was then repeated and the volume of water used was adjusted to give solution in which $[NT] \approx 10^{10}$ NTs mL^{-1} and $[CTAB] = 20$ mM (determined form the known initial concentration of CTAB and known volumes in subsequent sedimentation/redispersion steps). This solution is referred to as "CTAB-stabilized NTs". A portion of the CTAB-

stabilized NTs was then functionalized with TMA thiol by adding a small volume of concentrated thiol solution to the NTs ([TMA] = 20 mM) and stirring for 24 h to allow TMA to displace CTAB surfactant. Following functionalization, the NTs were washed with excess deionized water, allowed to sediment overnight, and then redispersed in deionized water such that [NT] $\approx 10^{10}$ NTs mL^{-1} and [CTAB] $\approx$ 0.5 mM. This solution is referred to as "TMA NTs". Finally, "TMA NTs with excess CTAB" was prepared by adding a small aliquot of concentrated CTAB to TMA NTs.

Mono and multilayers were prepared by depositing 4 μL of various NTs solutions (CTAB-stabilized NTs, TMA NTs, or TMA NTs with excess CTAB) onto solid substrates (Si, Si/SiO_2, AuTMA, AuMUA). Atomically flat {100} silicon wafers were purchased from Montco Silicon Technologies. SiO_2 surfaces were prepared by oxidizing silicon wafers in a plasma cleaner. TMA substrates were prepared by thermal evaporation of gold onto atomically flat silicon and subsequent functionalization of the gold using an ethanolic solution of excess TMA thiol. The wafer was then washed with acetone and methanol to remove any residual unbound TMA thiol. MUA substrates were prepared analogously and washed with a NaOH solution (pH $\approx$ 12) prior to NT deposition to deprotonate the MUA on the surface.

Received: April 29, 2010
Published online: August 16, 2010

Keywords: electrostatic interactions · nanostructures · Raman spectroscopy · self-assembly

[1] J. Grunes, J. Zhu, E. A. Anderson, G. A. Somorjai, *J. Phys. Chem. B* **2002**, *106*, 11463.
[2] S. A. Maier, P. G. Kik, H. A. Atwater, S. Meltzer, E. Harel, B. E. Koel, A. A. G. Requicha, *Nat. Mater.* **2003**, *2*, 229.
[3] M. Zayats, A. B. Kharitonov, S. P. Pogorelova, O. Lioubashevski, E. Katz, I. Willner, *J. Am. Chem. Soc.* **2003**, *125*, 16006.
[4] A. Guerrero-Martinez, J. Perez-Juste, E. Carbo-Argibay, G. Tardajos, L. M. Liz-Marzan, *Angew. Chem.* **2009**, *121*, 9648; *Angew. Chem. Int. Ed.* **2009**, *48*, 9484.
[5] T. Ming, X. S. Kou, H. J. Chen, T. Wang, H. L. Tam, K. W. Cheah, J. Y. Chen, J. F. Wang, *Angew. Chem.* **2008**, *120*, 9831; *Angew. Chem. Int. Ed.* **2008**, *47*, 9685.
[6] E. V. Shevchenko, D. V. Talapin, N. A. Kotov, S. O'Brien, C. B. Murray, *Nature* **2006**, *439*, 55.
[7] D. V. Talapin, E. V. Shevchenko, M. I. Bodnarchuk, X. C. Ye, J. Chen, C. B. Murray, *Nature* **2009**, *461*, 964.
[8] D. V. Talapin, J. S. Lee, M. V. Kovalenko, E. V. Shevchenko, *Chem. Rev.* **2010**, *110*, 389.
[9] K. J. M. Bishop, B. A. Grzybowski, *ChemPhysChem* **2007**, *8*, 2171.
[10] A. M. Kalsin, M. Fialkowski, M. Paszewski, S. K. Smoukov, K. J. M. Bishop, B. A. Grzybowski, *Science* **2006**, *312*, 420.
[11] A. M. Kalsin, B. A. Grzybowski, *Nano Lett.* **2007**, *7*, 1018.
[12] B. Kowalczyk, A. M. Kalsin, R. Orlik, K. J. M. Bishop, A. Z. Patashinskii, A. Mitus, B. A. Grzybowski, *Chem. Eur. J.* **2009**, *15*, 2032.
[13] S. Y. Park, A. K. R. Lytton-Jean, B. Lee, S. Weigand, G. C. Schatz, C. A. Mirkin, *Nature* **2008**, *451*, 553.
[14] S. C. Glotzer, M. J. Solomon, *Nat. Mater.* **2007**, *6*, 557.
[15] K. J. M. Bishop, C. E. Wilmer, S. Soh, B. A. Grzybowski, *Small* **2009**, *5*, 1600.
[16] F. M. van der Kooij, K. Kassapidou, H. N. W. Lekkerkerker, *Nature* **2000**, *406*, 868.
[17] R. Boyack, E. C. Le Ru, *Phys. Chem. Chem. Phys.* **2009**, *11*, 7398.
[18] B. Nikoobakht, J. P. Wang, M. A. El-Sayed, *Chem. Phys. Lett.* **2002**, *366*, 17.
[19] S. B. Chaney, S. Shanmukh, R. A. Dluhy, Y. P. Zhao, *Appl. Phys. Lett.* **2005**, *87*, 3.
[20] S. M. Nie, S. R. Emery, *Science* **1997**, *275*, 1102.
[21] E. Hao, G. C. Schatz, *J. Chem. Phys.* **2004**, *120*, 357.
[22] D. Witt, R. Klajn, P. Barski, B. A. Grzybowski, *Curr. Org. Chem.* **2004**, *8*, 1763.
[23] R. D. Deegan, O. Bakajin, T. F. Dupont, G. Huber, S. R. Nagel, T. A. Witten, *Nature* **1997**, *389*, 827.
[24] T. P. Bigioni, X. M. Lin, T. T. Nguyen, E. I. Corwin, T. A. Witten, H. M. Jaeger, *Nat. Mater.* **2006**, *5*, 265.
[25] J. E. Millstone, W. Wei, M. R. Jones, H. J. Yoo, C. A. Mirkin, *Nano Lett.* **2008**, *8*, 2526.
[26] D. J. Harris, H. Hu, J. C. Conrad, J. A. Lewis, *Phys. Rev. Lett.* **2007**, *98*, 4.
[27] Higher concentrations of CTAB could not be investigated as the amount of residual organics becomes too large for the NTs to be imaged by SEM.
[28] MUA-functionalized AuNTs were not prepared, as the interactions between negatively charged MUA and the positively charged hexadecyltrimethylammonium bromide (CTAB) surfactant (which stabilizes the as-synthesized AuNTs) leads to rapid and irreversible aggregation of the triangles.
[29] E. J. W. Verwey, J. T. G. Overbeek, *Theory of Stability of Lyophobic Colloids*, Elsevier, Amsterdam, **1948**.
[30] G. B. Irani, T. Huen, F. Wooten, *J. Opt. Soc. Am.* **1971**, *61*, 128.
[31] R. J. Hunter, *Foundations of Colloid Science*, *2nd ed.*, Oxford University Press, New York, **2001**.
[32] Our estimates of electrostatic energies neglect edge effects due to finite sizes of the triangles. We note, however, that because of screening, electrostatic forces are relatively-short ranged ($\kappa^{-1} \approx 5$ nm),[15] the edge effects are negligible (at most 12% of the total electrostatic energy).
[33] Charge density was calculated from the electrophoretic mobility, as determined by a Malvern Zetasizer Nano-ZS instrument. Given the size of our particles, the relation between mobility and surface charge density can be approximated by[31] $\sigma = \mu\nu\kappa$, where μ is the mobility, ν is the viscosity of the medium, and κ^{-1} is the electrostatic screening length of a given solution.
[34] The gravitational length scale for our system, $L_g = kT/m_{NT}g \approx 0.2$ mm (m_{NT} is the mass of one NT and g is the acceleration due to gravity) is commensurate with the height of the droplet during evaporation (0.1–1 mm). Therefore, the NTs form a suspension that is not thermodynamically stable.
[35] A. J. Haes, J. Zhao, S. L. Zou, C. S. Own, L. D. Marks, G. C. Schatz, R. P. Van Duyne, *J. Phys. Chem. B* **2005**, *109*, 11158.
[36] L. J. Sherry, R. C. Jin, C. A. Mirkin, G. C. Schatz, R. P. Van Duyne, *Nano Lett.* **2006**, *6*, 2060.
[37] A. J. Haes, R. P. Van Duyne, *J. Am. Chem. Soc.* **2002**, *124*, 10596.
[38] K. L. Kelly, E. Coronado, L. L. Zhao, G. C. Schatz, *J. Phys. Chem. B* **2003**, *107*, 668.
[39] L. D. Qin, S. L. Zou, C. Xue, A. Atkinson, G. C. Schatz, C. A. Mirkin, *Proc. Natl. Acad. Sci. USA* **2006**, *103*, 13300.
[40] Herein we report the relative change in SERS enhancement factors associated with the ordering of NTs (i.e., SERS enhancement factor of ordered NTs/SERS enhancement factor of disordered NTs), not the value of the SERS enhancement factor itself. Determination of the SERS enhancement factor for each individual system is not plausible because neither the exact concentration of MB on the NT substrate after evaporation nor the fraction of the surface area that is "active" upon irradiation of the multilayer NT crystals are known. Without knowing these individual enhancement factors it is impossible to compare directly the absolute enhancement of this system with systems of other morphologies.
[41] D. K. Smith, N. R. Miller, B. A. Korgel, *Langmuir* **2009**, *25*, 9518.

